applied sciences

MDPI

Article

Investigation of Acoustic Emission of Cracks in Rails under Loading Close to Operational

Vera Barat [1,2,*], Artem Marchenkov [1], Sergey Ushanov [1,2], Vladimir Bardakov [1,2] and Sergey Elizarov [2]

[1] Institute of Information Technologies and Computer Science, National Research University "Moscow Power Engineering Institute", Krasnokazarmennaya Str., Moscow 111250, Russia
[2] LLC Interunis-IT, Shosse Entuziastov 20B, Moscow 111240, Russia
* Correspondence: vera.barat@mail.ru

Abstract: The paper is devoted to the study of the possibility of detecting cracks in railway rails by the acoustic emission (AE) method. An experimental study of AE signals under cyclic compression loading of rail fragments, which simulates the rail operating load, has been carried out. Fragments of rails without defects, as well as fragments containing pre-grown fatigue cracks, were studied. It was found that AE signals generated by a rail with a crack have higher activity compared to signals from defect-free specimens. It is shown that the AE signals during the loading of defect-free specimens have a short duration and low amplitude and may be caused by the deformation of non-metallic inclusions. The crack presence leads to an increase in the AE hits rate and changes the nature of the distribution of the AE hits amplitudes. It is shown that the crack location has no effect on the reliability of its detection by the AE method. Criteria of crack detection by AE testing are offered as a result of this study.

Keywords: acoustic emission; rail; crack; defect; crack detection

Citation: Barat, V.; Marchenkov, A.; Ushanov, S.; Bardakov, V.; Elizarov, S. Investigation of Acoustic Emission of Cracks in Rails under Loading Close to Operational. *Appl. Sci.* **2022**, *12*, 11670. https://doi.org/10.3390/app122211670

Academic Editor: Giuseppe Lacidogna

Received: 5 October 2022
Accepted: 15 November 2022
Published: 17 November 2022

1. Introduction

High-speed railway has significantly developed in the world recently. Meanwhile, researchers pay more attention to rail safety problems [1]. Many studies were carried out to ensure rail safety to detect rail cracks by acoustic emission (AE) technology. Compared with the other traditional detection methods, the AE method has the advantages of progressive type defects detection, unlimited geometric shape, high sensitivity, and real-time monitoring [2,3]. At present, many papers devoted to the study of the AE method applied to rail defects detection have been published so far. Research is successfully carried out both with the help of laboratory stands simulating elements of rail structures and within the framework of full-scale field experiments. The most relevant areas of research are the study of the regularities of AE generation during the propagation of cracks in rail steels, the identification of AE hits against the noise background associated with rail-wheel contact, as well as identification of railway wheels and rails damage using the AE method.

The fundamental possibility of the AE method application for rail defects detection was shown in [4,5]. The authors found that rail defects under loading states close to operational ones are sources of AE, and the possibility of detecting AE signals against noise background was also investigated. In [6–8], the intensity of contact stresses between the wheel and the rail is estimated using the parameters of continuous AE. Based on the assessment of the rail degree of wear, the rail residual life was estimated. Friction, vibration, and shock arising from the contact between the wheel and rail create high-level transient noise, which can significantly complicate the process of AE diagnostics. However, noise and useful AE signals have different natures and differ in waveform and spectrum. The authors in [9,10] found that AE hits can be detected against the noise background based on a broadband spectrum and on a small rise time and duration. The difference in the scale of the noise and the useful signals makes it possible to identify AE hits corresponding

to defects in rail structure, based on the wavelet decomposition of the AE data. Various modifications of the wavelet transform are used—wavelet packets [11], continuous [2], and discrete wavelet transform. In [3,12], optimal wavelet bases are constructed based on the AE signal's waveform. After the wavelet decomposition of detected AE hits, criteria based on a comparative analysis of the various wavelet coefficients entropy are applied [13].

Also, classification methods, both statistical and based on the use of neural networks, are effectively used to identify AE hits associated with various types of rail defects. The classification is used to determine hazardous and non-hazardous states of the system based on characteristic AE patterns or to identify useful AE signals against the noise background. Thus, in [14], the degree of danger of the detected defects is determined using the Chebyshev inequality, which makes it possible to establish the correspondence of the AE data to certain characteristic patterns of rail elastic and plastic deformation. In [15], to determine the defectiveness of a rail, Bayesian regression of the frequency parameter characterizing the structural state of the material is used. As a rule, self-organizing networks are used as neural networks, for example. In [16,17], a convolutional neural network is used to identify signals corresponding to various sources: noise caused by train movement, wheel impacts on the rail, and defects as sources of acoustic emission. In [18], within the framework of deep learning technology, a Long Short Term Memory network is used, which is trained on a representative sample of noises, and then detects signals of a nontypical waveform, which at the next stage of the algorithm, based on a set of specific features, can be classified as AE hits corresponding to defects. Analysis of the publication activity on various topics related to AE diagnostics of rails reveals that most of the papers are devoted to data science issues, namely, data filtering and the identification of useful signals against the noise background. At the same time, the number of studies devoted to the analysis of the laws of acoustic emission during the development of cracks in rail steels and the characteristics of a rail fatigue crack as an AE source is rather limited. Researchers in [5] investigated the effectiveness of the AE method in detecting crack initiation and growth in rail specimens exposed to bending, and the success rate for detecting the onset of crack progression was 100%. A more detailed analysis of AE data is given in [19,20], where the potential of the AE method for online monitoring of rail crack progression under traffic loading was explored by carrying out laboratory tests on rail segments subjected to vertical loading in the presence of machine noise and specimen deformation. The paper notes that high amplitude AE hits are associated with material deformation processes even before the crack onset was observed. The authors analyze the shape and spectrum of AE signals and identify groups of AE hits associated with various deformation mechanisms of rail steel. In [21], the authors estimate the length of a fatigue crack on the basis of AE data. For this, at the first stage, the AE signals associated with the friction of the crack faces are detected. The crack length is estimated by a regression model, which is based on the spectral parameters of the friction signals.

Some very useful approaches to identifying rail defects can be borrowed from bearing diagnostics. Analogies between these objects are possible since shock loads, friction, and wear play the main role in the occurrence of cracks in both cases.

Papers [22,23] seem to be the most interesting. In one study [22], the spectra of AE signals corresponding to various wear mechanisms are presented. In another study [23], the patterns of changes in the AE parameters during the crack growing are presented.

Within the current research framework, an experimental study of the acoustic emission of rail cracks under loading is carried out, simulating the operation mode when a train passes. The configuration of the specimens, the size of the cracks, and the magnitude of the applied load were chosen in such a way that the deformation of the specimen predominantly corresponded to the elastic region of the tensile diagram. Under such conditions, in the absence of critical defects and significant plastic deformation, the diagnostic task is complicated due to the lower AE hits rate of the defect and a decrease in the level of the AE hits amplitudes compared with the pre-destructive states. The article provides a

quantitative analysis of the AE parameters and detection of the hits corresponding to the defect against the background of structural noise arising from the deformation of the rail.

2. Materials and Methods

Railroad rail R43, manufactured from E76F high-carbon steel, was chosen as the object under study. The chemical composition and mechanical properties of E76F high-carbon steel are presented in Tables 1 and 2, respectively.

Table 1. E76F steel chemical composition (reference data).

Steel	The Content of Chemical Elements (% wt.)						
	C	**Mn**	**Si**	**V**	**Al**	**S**	**P**
E76F	0.71–0.82	0.75–1.15	0.25–0.6	0.03–0.15	≤0.02	≤0.025	≤0.025

Table 2. E76F steel mechanical properties (evaluated by tension test).

Parameter	Mean Value
Offset yield strength, MPa	428
Ultimate tensile stress, MPa	839
Elongation to rupture, %	7.5

The tested specimens were in the form of rail fragments with a thickness of 10 ± 1 mm. After cutting, the surfaces of the fragments were milled and ground to obtain the appropriate surface quality. On the cut fragments, thin notches were made over the entire thickness of the rail at a defined depth, simulating a defect. The width of the finished notch is between 0.25 and 0.3 mm. The notch depth is between 2 and 4 mm, depending on the specimen. Specimens with three different notch locations were investigated: in the rail web, in fillet transitions from the rail web to the head, and from the web to the foot. A photograph of one of the rail fragments with a notch in the web is shown in Figure 1a. A fatigue crack of a defined length was grown on the notched rail fragments by means of the Instron 8801 testing machine (Figure 1b). Smooth cyclic loading was performed by compression with a sinusoidal cycle with a frequency of 10 Hz and a cycle asymmetry coefficient R = 0. The length of the cracks was between 0.5 and 2.5 mm.

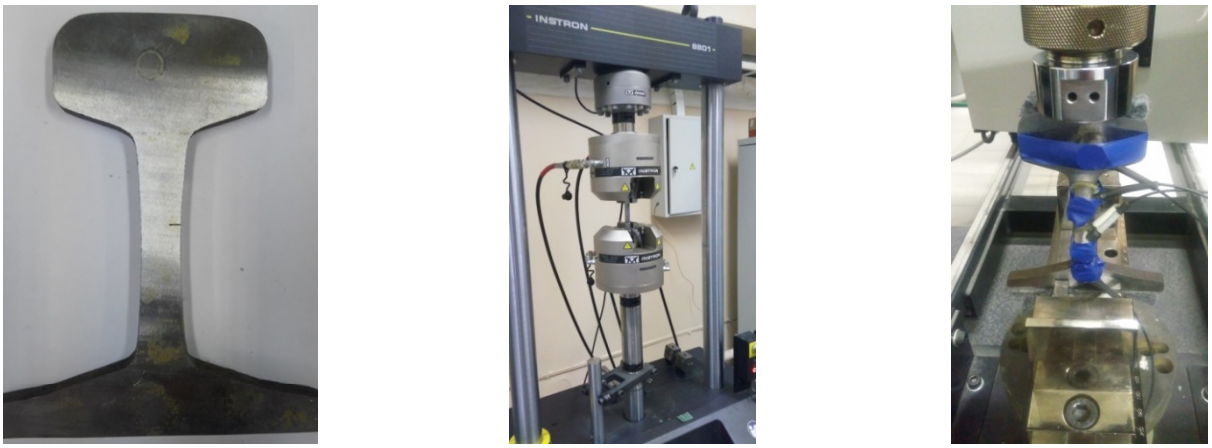

(**a**) (**b**) (**c**)

Figure 1. Rail fragment (**a**); fatigue crack growing in Instron 8801 testing machine (**b**); test of the prepared fragment (**c**).

Testing of rail specimens with a notch and fatigue crack was carried out on an Instron 5982 universal testing machine in compression loading mode. An in-situ photograph of the specimen during the experiment is shown in Figure 1c.

Figure 2 shows the frequency response of the AE sensor GT200 used in the experiment. The sensor has high sensitivity in the frequency band of 50–200 kHz, with the highest transformation coefficient at a frequency of about 180 kHz. Even though the sensor is resonant, its sensitivity remains relatively high (about 40–50 dB) in the high-frequency region, which makes it possible to register AE signals in the frequency range of 300–400 kHz.

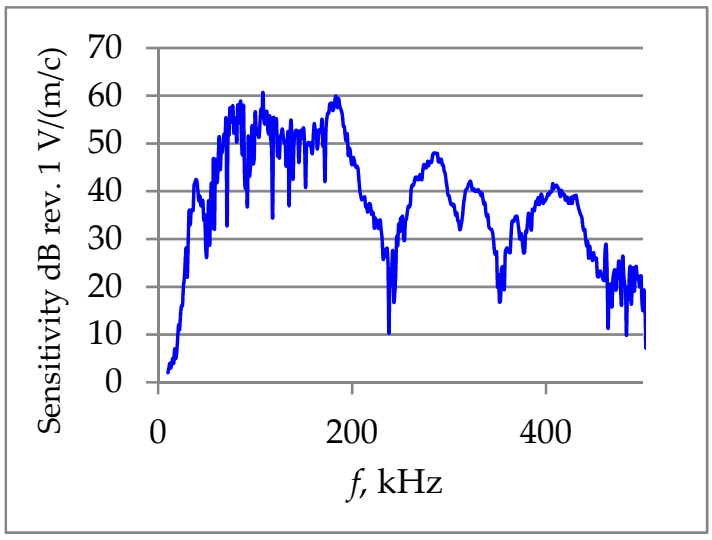

Figure 2. Frequency response of AE sensor GT200.

The loading of the specimen was carried out by cyclic compression according to a programmed cycle (see Figure 3), simulating the passage of a train carriage at a low speed (between 3 and 4 km/h) with maximum cycle stress of 15, 30, and 45 kN. Each rail was loaded with 120 cycles, which approximately corresponds to the loading of the rail during train travel.

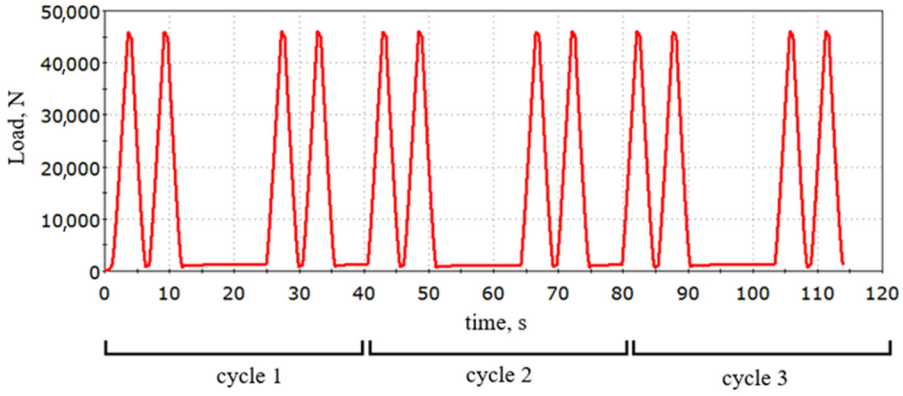

Figure 3. Cyclorama for testing rail fragments with a maximum load of 45 kN.

AE signals were registered during the tests using the industrial system A-Line DS (produced by LLC "INTERUNIS-IT"). The measuring chain consisted of resonant AE sensor GT200 (with 180 kHz resonant) and preliminary digital amplifiers ALS with 26 dB gain coefficient (produced by LLC "INTERUNIS-IT"). The intrinsic noise of the equipment, preamplifier, and sensor was 20 dB. The acoustic peak background noise level after placing the specimen in the grips of the testing machine was 30 dB, and the amplitude discrimina-

tion threshold was set equal to 45 dB. The data acquisition used a 100–500 kHz digital filter to exclude the noise of the testing machine.

Metallographic studies, which were carried out to identify the microstructure features of the rail material, were performed on microsections cut in the longitudinal and transverse directions. Microstructure studies were carried out using optical microscopy at magnifications of 100x–1000x on a Zeiss Observer Z1m microscope. Studies of non-metallic inclusions were carried out on a Tescan Vega 3 scanning electron microscope using the EDX (energy-dispersive X-ray spectroscopy) as a surface elemental analysis method.

Since the amplitude and waveform parameters of AE hits are random variables, statistical methods are used to identify patterns. Since one of the diagnostic criteria of the AE method is the correspondence of data to a certain type of distribution, in this paper, we use the χ^2 goodness-of-fit test, which allows us to establish the correspondence of the empirical distribution to a certain theoretical law. The criterion is calculated using Equation (1)

$$\chi^2 = \sum_{i=1}^{k} \frac{(F_i - f_i)^2}{f_i} \quad (1)$$

where k—number of intervals for the parameter under study, F_i and f_i—theoretical and empirical probability for each observation interval.

Various types of statistical graphs are also used during AE data analysis—histograms and scatterplots, which allow exploring data in a two-dimensional feature space, as well as variability plots that allow for comparison of the average values and variation of informative parameters for different types of objects.

3. Results and Discussion

When testing defect-free rail specimens, AE hits with amplitudes of 45–55 dB were registered, and the dependence of the amplitude values on time in accordance with the applied load is shown in Figure 4. AE hits were registered mainly in the phase of increasing load with the uniform activity of no more than 25–30 hits per cycle (or 2–5 hits per second).

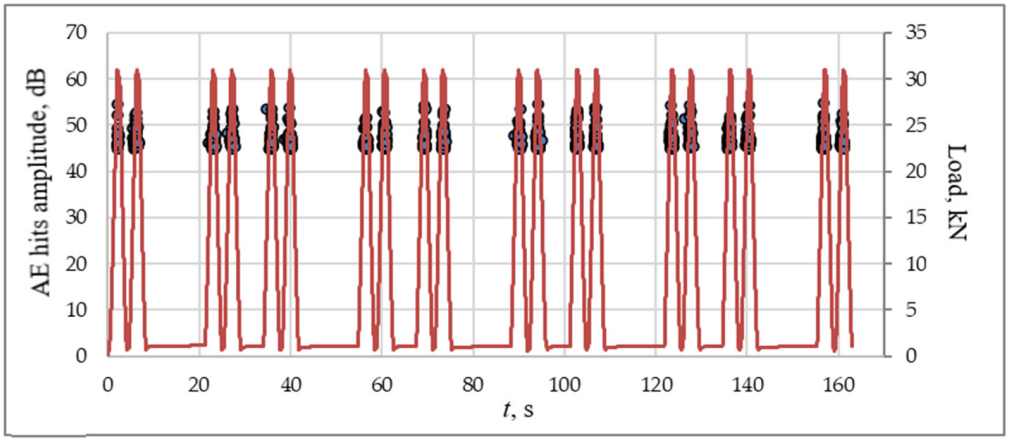

Figure 4. Dependence of AE hits amplitudes on time (blue) and dependence of loading force on time (red) for defect-free specimen.

During the loading of defect-free specimens, the more reasonable sources of AE activity seem to be various external noises. However, the waveform and spectrum of the measured signals indicate that the AE source has a microscopic size and is located inside the specimen. All signals have a repeatable waveform with a low duration between 50 and 150 µs (Figure 5a,c). At that, two types of frequency spectrums were registered (Figure 5b,d). AE waveforms are presented without gain coefficient compensation. In 80% of cases, the spectrum has a resonance character in the frequency band 100–200 kHz near the resonant frequency of the sensor (Figure 5b). In 20% of other cases, the spectrum

contains a high-frequency part in the region 300–450 kHz (Figure 5d). The waveform and spectrum of AE signals shown in Figure 5 are similar to a signal represented in [20], which are generated by cyclic loading of specimens from rail steel on the stage before the crack onset. We can conclude that during elastic deformation of a defect-free specimen, observed AE corresponds to deformation of the inner structure of the material, i.e., a kind of "structural noise" of the testing object is formed.

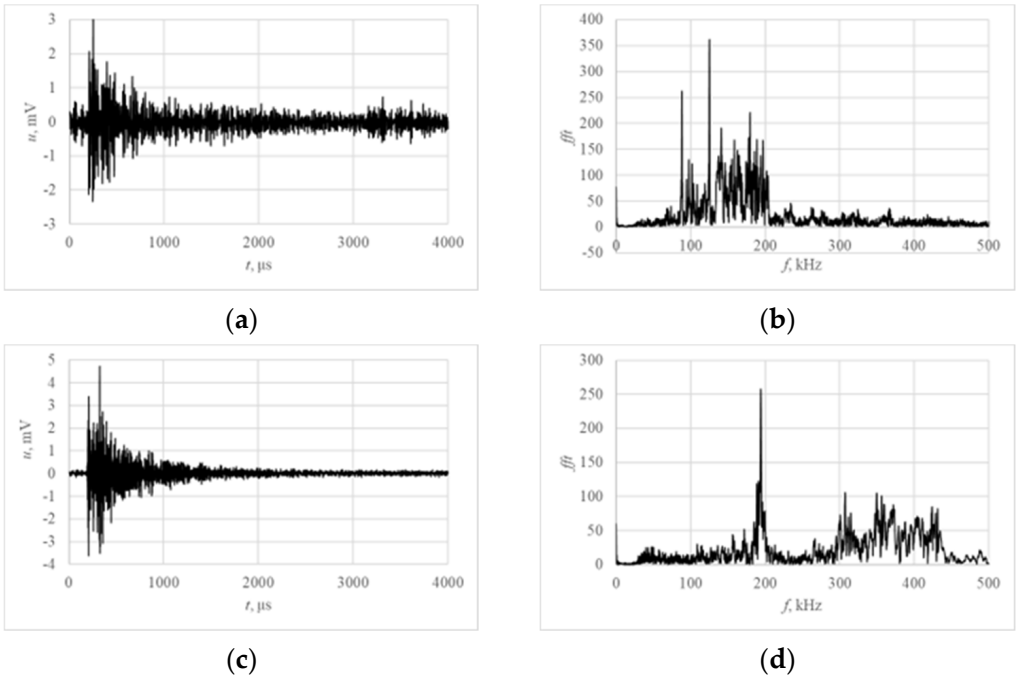

Figure 5. Typical waveform (**a**,**c**) and spectrums (**b**,**d**) of AE signals obtained during the loading of defect-free specimens.

The short duration and fast rise time of the AE signals exclude internal noise as a probable cause of AE generation. It is known that the short scale of the signals corresponds to the short scale of the process, that typical for a source of AE [24]. The fast rise time could be evidence of the rapid release of elastic energy, which is typical for the destruction processes. Such signals are not typical for external noises like friction, vibration, and the noise of the testing machine.

The effect of "structural noise" from porous collapse in granular Mg-Ho alloys has been investigated in the fundamental works [25,26], and the AE hits corresponding to this process have been characterized and identified with specific values of AE hit amplitudes. A study [27,28] noted that the appearance of AE hits with a short rise time can also be caused by the deformation of the cementite in the structure of high-carbon steel. AE signals similar in waveform to those shown in Figure 5 were obtained in [29] at the elastic deformation stage; the authors explain the appearance of such signals by welding inclusions in the material structure.

A study of the microstructures of rail steel specimens was carried out to identify possible sources of structural noise. The microstructure of the rail consists of quasi-eutectoid pearlite grains along the boundaries of which the ferrite phase is located (see Figure 6a). At the same time, in the study of non-etched microsections, non-metallic inclusions elongated in the rolling direction were revealed (Figure 6b). The SEM study of the rail fracture made it possible to establish that most non-metallic inclusions are manganese sulfides MnS (Figure 6c,d) and complex manganese silicates $2MnO{\cdot}SiO_2$. It is known that inclusions of manganese sulfides in pearlitic steels can significantly affect the activity of acoustic emission under loading even in the elastic region [30], so we associate the appearance of such signals with a debonding or cracking of these inclusions.

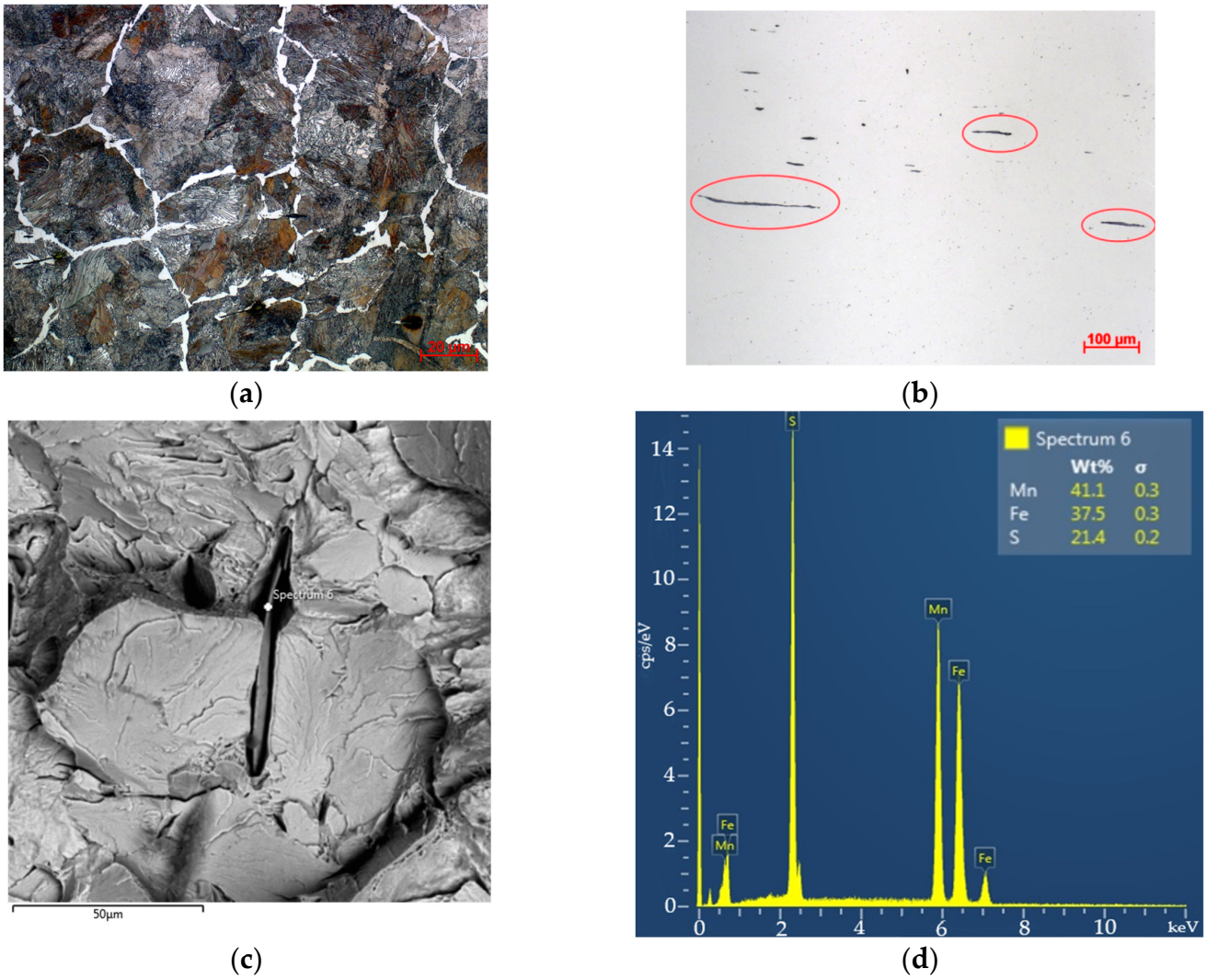

(**a**) (**b**)

(**c**) (**d**)

Figure 6. Rail microstructure (**a**) and non-metallic inclusions (highlighted in red) in the longitudinal section (**b**); photograph (**c**) and EDX-spectrum (**d**) of a nonmetallic sulfide inclusion revealed in a fracture of a rail fragment by EDX-analysis.

Figure 7 shows typical distributions of amplitudes for different maximum cycle stress values: 15, 30, and 45 kN, respectively. The distribution of AE hits amplitudes for all specimens predominantly (in more than 90% of cases) corresponds to an exponential law, which is confirmed using the χ^2 goodness of fit criterion, with a p-value exceeding 0.05. In the opinion of most researchers [31], an exponential distribution is characteristic of the stage of diffuse fracture of the material preceding the formation of a macroscopic defect, which also confirms the hypothesis of structural noise [20].

When testing a specimen with a pre-grown crack, hits with an amplitude of up to 80 dB were recorded (Figure 8). Another difference from the data obtained when loading a defect-free specimen is that AE hits are recorded both with increasing and decreasing load.

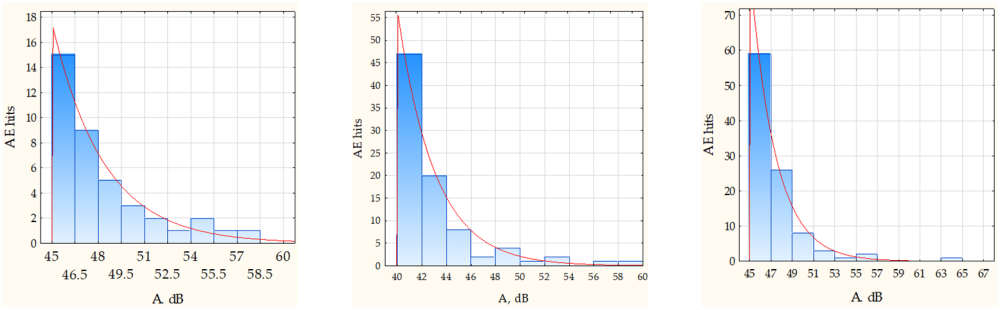

(**a**) (**b**) (**c**)

Figure 7. Distribution of AE hits amplitudes for a defect-free specimen at various load values 15 kN (**a**) 30 kN (**b**) 45 kN (**c**).

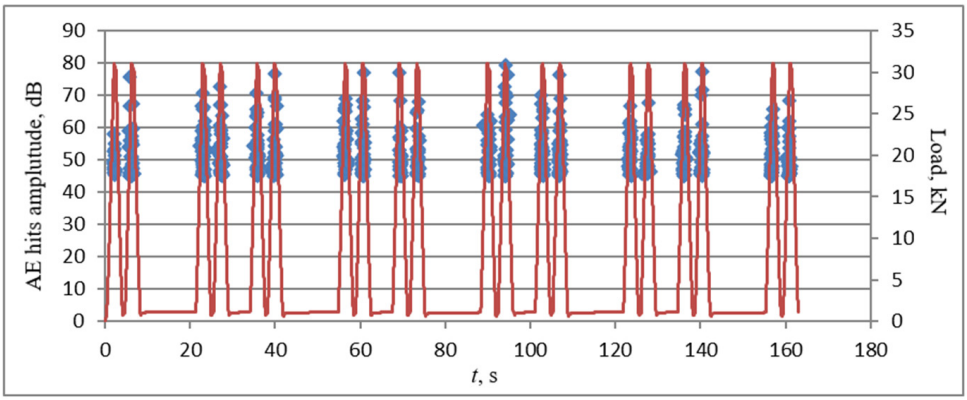

Figure 8. Dependence of AE hits amplitudes on time (blue) and dependence of loading force on time (red) for defective specimen.

In addition to signals of small amplitude and duration, similar in waveform and spectrum to the signals shown in Figure 5, while testing specimens with a defect, signals with a specific waveform are also recorded. For example, signals that have a longer decay time and, therefore, a longer duration of the order of several milliseconds (Figure 9a,b), as well as narrow-band signals with amplitude modulation, the source of which may be the friction of the crack edges (Figure 9c,d). AE waveforms are presented without gain coefficient compensation.

The appearance of a crack leads to a change in the law of the probability distribution of AE hits amplitudes; for a specimen with a crack, the distribution of amplitudes in each loading cycle corresponds to the half-normal law. Figure 10 shows typical distributions of amplitudes at various values of the load, and red graphs correspond to the theoretical distribution law.

In the presence of a defect, the amplitude distribution tends to be normal in comparison with a defect-free specimen. This phenomenon could be explained due to the presence of several independent AE sources, such as the structural noise of an object, crack growth, and friction of its edges. Compliance with the half-normal law is determined reliably using the χ^2 test in 78% of cases with a p-value of more than 0.05.

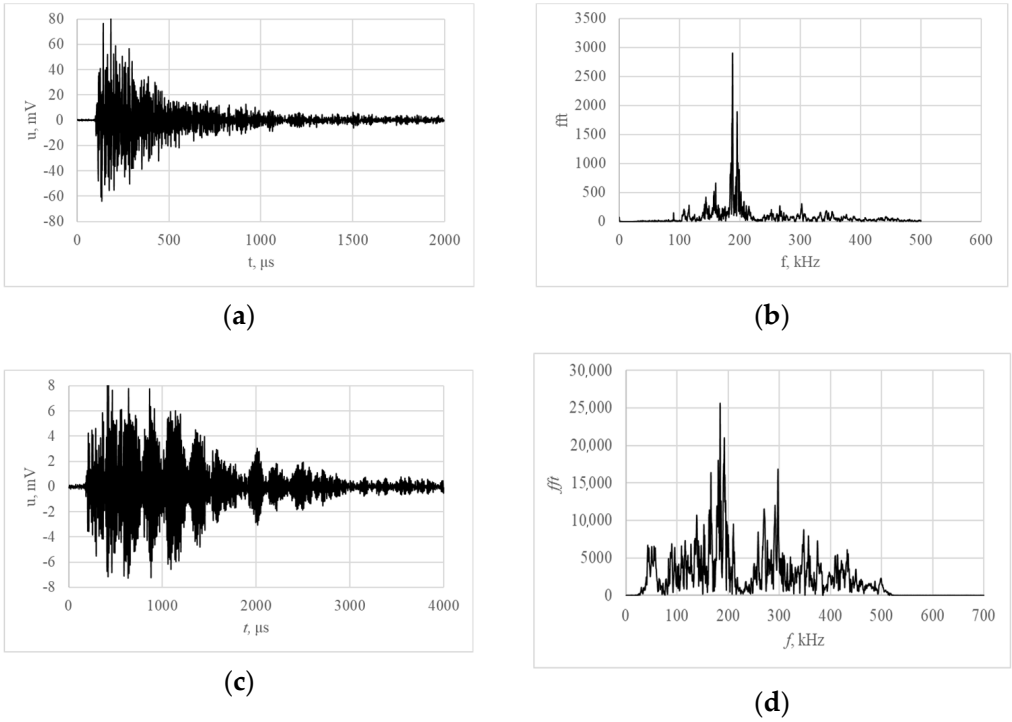

Figure 9. Typical waveform (**a**,**c**) and spectrums (**b**,**d**) of AE signals obtained during the loading specimens containing crack.

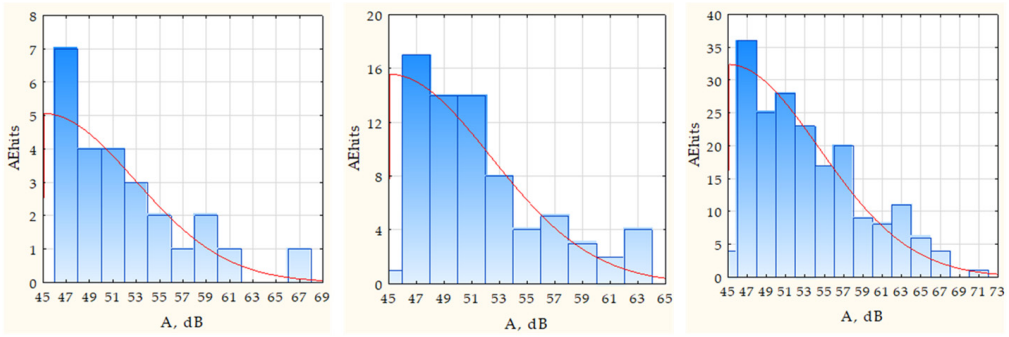

Figure 10. Distribution of AE hits amplitudes for a specimen with defect at various load values 15 kN (**a**); 30 kN (**b**); 45 kN (**c**).

When testing specimens with different sizes and locations of cracks, significant variability of the data was observed. The proportion of high-amplitude AE hits was different for different specimens, and the AE hits rate was manifested to a different extent. AE data parameters recorded during experiments for defect specimens (with different defect locations) and for defect-free specimens are shown in Table 3. Since the main task of data analysis is the separation of defective and defect-free specimens, the AE hits rate, expressed in the number of AE hits per loading cycle, and the quantile of the amplitude distribution of the order of 0.9, characterizing the distribution tail, were considered as descriptors.

Table 3. Values of AE parameters obtained during testing.

Defect Location	Specimen	Average Number of Hits			Quantile $q_{0.9}$		
		15 kN	30 kN	45 kN	15 kN	30 kN	45 kN
no defect	R1	1	9	21	50.8	50.2	50.9
	R2	3	13	11	52.2	53.5	54.9
	R3	2	13	18	52.6	54.3	53.3
	R4	3	12	23	52.0	52.8	54.4
mean		2.3	11.8	17.5	51.9	52.7	53.4
web	R5	3	24	45	51.3	53.9	56.3
	R6	4	7	37	52.3	57.1	57.5
	R7	4	11	44	53.3	57.7	58.2
	R8	2	12	39	52.5	58.3	59.6
	R9	2	19	34	53.7	57.5	60.3
mean		3.14	16.43	41.00	52.71	56.86	58.36
web-head	R10	2	14	29	49.9	55.4	56.9
	R11	2	33	47	53.2	55.1	57.8
	R12	2	9	32	51.9	55.4	56.9
mean		2.0	18.7	36.0	51.7	55.3	57.2
web-foot	R13	2	31	36	52.5	59.1	59.8
	R14	5	14	19	52.6	57.7	59.7
	R15	4	12	33	52.6	58.1	59.4
mean		3.7	19.0	29.3	52.9	58.3	59.6

Parameters represented in Table 3 show that the AE hit rate and amplitudes of AE hits increased when the load was increasing. At a load of 15 kN, the activity and energy of AE hits are low for both defective and defect-free specimens. Still, with a load rise, an increase in the AE hit rate is manifested to a greater extent for defective specimens than for defect-free specimens.

It should also be noted that there is a significant difference in the AE parameter values corresponding to defective and defect-free specimens. At the maximum load value equal to 45 kN, the number of AE hits recorded per loading cycle for defect-free specimens is, as a rule, no more than 20 AE hits per loading cycle. In contrast, for defective specimens, the AE hits rate, as a rule, turns out to be 1.5–2 times higher. The amplitude distribution quantile $q_{0.9}$ for specimens with a defect is 4 dB higher than for defect-free specimens, which increases the proportion of high-amplitude signals in the data sample.

However, for specimens with different crack locations and for different crack lengths, a pronounced difference in the AE data is not observed; Figure 11 shows the variability plots, which show the scatter of the AE parameters for different locations of cracks. Analysis of the data depicted in Figure 11 shows that for groups of specimens with different locations of the crack, the intragroup dispersion turned out to be greater than the intergroup dispersion. Therefore, the location of the crack does not affect the reliability of its detection by the AE testing.

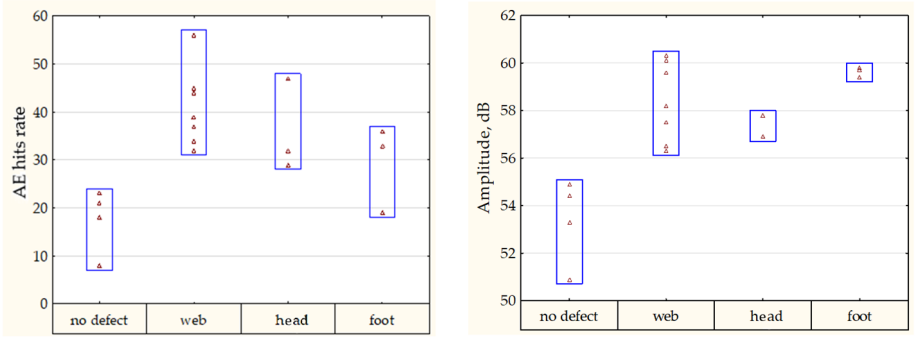

(**a**) (**b**)

Figure 11. Variability plots for AE hit rate (**a**) and quantile $q_{0.9}$ of amplitude distribution (**b**) for specimens with different crack locations.

Since the presence of a crack leads to the appearance of AE signals of greater amplitude and duration, most clearly, AE data corresponding to defective and defect-free specimens differ in the correlation graph showing the relationship between the AE hits duration and its amplitude. Three areas can be distinguished on the correlation plane. Area 1, corresponding to the noise of the loading machine and contact friction, is empty (excluding the intersecting part of regions 1 and 2, which corresponds to region 2) since these types of noises are filtered parametrically and mechanically due to the introduction of damping pads made of acoustic felt. In region 2, signals of low amplitude and duration are localized, which can be identified as structural noise of rail steel caused by the presence of non-metallic inclusions and deformation of the cementite network in the material structure. The signals associated with the development of a crack are localized in region 3. In this region, there is a pronounced difference in the graphs corresponding to defective and defect-free specimens.

Table 4 shows the values of the parameter N_3 corresponding to the number of indications in area 3 of scatterplots (Figure 12) for defective and defect-free samples. Analysis of the data given in Table 4 shows that the values corresponding to defective and defect-free specimens differ significantly from each other.

Table 4. The values of the criterion parameter N_3.

Specimen Number	R1	R2	R3	R4	R5	R6	R7	R8	R9	R10	R11	R12	R13	R14	R15
Number of AE hits N_3	7	12	8	3	46	64	31	56	29	34	74	45	61	43	35

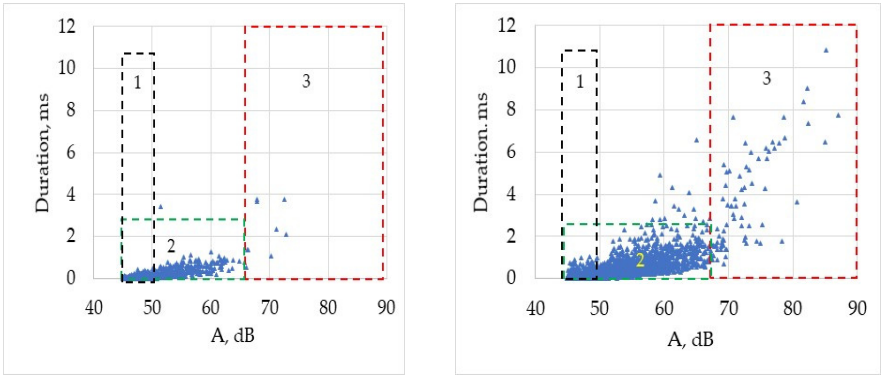

(**a**) (**b**)

Figure 12. Scatterplots AE hit durations vs. AE hit amplitudes for defect-free specimens (**a**) and for defective specimens (**b**). Area 1 localized noise of the loading machine (black rectangle), area 2—structural noise (green rectangle), area 3—defects (red rectangle).

4. Conclusions

Within the framework of this research, the study of fatigue cracks acoustic activity in specimens made of rail fragments under loading, simulating the passage of a train, was carried out. Fragments of rails without defects, as well as fragments containing pre-grown fatigue cracks in different locations of samples, were studied.

While testing defect-free specimens, even after eliminating all external noise sources, AE signals were recorded, the most probable cause of which is the deformation and cracking of non-metallic inclusions of the material [24]. AE signals obtained during the testing of defect-free specimens have a short duration and amplitudes of up to 60 dB. Their amplitude distribution corresponds to an exponential law with a high degree of reliability.

The appearance of a crack leads to an increase in the AE hits rate and a change in the nature of the distribution of AE hits amplitudes. The presence of several AE sources associated with crack growth, the friction of the edges, as well as the presence of structural noise leads to the normalization of the AE hits amplitudes distribution law. The AE hits rate corresponding to the growth and friction of the crack edges is about 30–40 hits per loading cycle that, simulates the passage of a wheel, and the amplitudes of the AE hits correspond to the range of 60–75 dB.

Author Contributions: All authors contributed to the study conception and design. Conceptualization: V.B. (Vera Barat) and A.M.; methodology, V.B. (Vera Barat) and A.M.; validation, V.B. (Vladimir Bardakov) and S.U.; formal analysis, S.U.; investigation, V.B. (Vera Barat) and A.M.; resources, S.E.; data curation, V.B. (Vera Barat) and S.U.; writing—original draft preparation, V.B. (Vera Barat); writing—review and editing, V.B. (Vladimir Bardakov); visualization, S.E.; supervision, S.E.; project administration, S.E. and A.M. All authors have read and agreed to the published version of the manuscript.

Funding: The reported study was funded by the Russian Foundation for Basic Research, Sirius University of Science and Technology, JSC Russian Railways, and Educational Fund "Talent and success" (project 20-38-51019).

Institutional Review Board Statement: Not applicable.

Informed Consent Statement: Not applicable.

Data Availability Statement: Not applicable.

Conflicts of Interest: The authors declare no conflict of interest.

References

1. Alahakoon, S.; Sun, Y.; Spiryagin, M.; Cole, C. Rail flaw detection technologies for safer, reliable transportation: A review. *J. Dyn. Syst. Meas. Control. -Trans. Asme* **2018**, *140*, 1–17. [CrossRef]
2. Zhang, J.; Ma, H.; Yan, W.; Li, Z. Defect detection and location in switch rails by acoustic emission and Lamb wave analysis: A feasibility study. *Appl. Acoust.* **2016**, *105*, 67–74. [CrossRef]
3. Hao, Q.S.; Zhang, X.; Wang, K.W.; Wang, Y.; Shen, Y. A signal-adapted wavelet design method for acoustic emission signals of rail cracks. *Appl. Acoust.* **2018**, *139*, 251–258. [CrossRef]
4. Bruzelius, K.; Mba, D. An initial investigation on the potential applicability of Acoustic Emission to rail track fault detection. *NDTE Int.* **2004**, *37*, 507–516. [CrossRef]
5. Bassim, M.; Lawrence, S.; Liu, C.D. Detection of the onset of fatigue crack growth in rail steel using acoustic emission. *Eng. Fract. Mech.* **1994**, *41*, 207–214. [CrossRef]
6. Thakkar, N.; Steel, J.; Reuben, R. Rail–wheel interaction monitoring using Acoustic Emission: A laboratory study of normal rolling signals with natural rail defects. *Mech. Syst. Signal Process.* **2010**, *24*, 256–266. [CrossRef]
7. Thakkar, N.; Steel, J.; Reuben, R. A laboratory study of rail-wheel interaction monitoring using acoustic emission: Effect of rolling conditions with and without lateral rattling. *Proc. Inst. Mech. Eng. Part F J. Rail Rapid Transit* **2013**, *227*, 161–175. [CrossRef]
8. Thakkar, N.; Steel, J.; Reuben, R. Rail-wheel contact stress assessment using acoustic emission: A laboratory study of the effects of wheel flats. *Proc. Inst. Mech. Eng. Part F J. Rail Rapid Transit* **2012**, *226*, 3–13. [CrossRef]
9. Zhang, X.; Sun, T.; Wang, K.; Wang, Y.; Shen, Y. A parameter optimized variational mode decomposition method for rail crack detection based on acoustic emission technique. *Nondestruct. Test. Eval.* **2020**, *36*, 411–439. [CrossRef]
10. Amini, A.; Entezami, M.; Huang, Z.; Rowshandel, H.; Papaelias, M. Wayside detection of faults in railway axle bearings using time spectral kurtosis analysis on high-frequency acoustic emission signals. *Adv. Mech. Eng.* **2016**, *8*, 1–9. [CrossRef]

11. Bianchi, D.; Mayrhofer, E.; Groschl, M.; Betz, G.; Vernes, A. Wavelet packet transform for detection of single events in acoustic emission signals. *Mech. Syst. Signal Process.* **2015**, *64*, 441–451. [CrossRef]
12. Zhang, X.; Feng, N.; Zou, Z.; Wang, Y.; Shen, Y. Acoustic emission detection of rail defect based on wavelet transform and Shannon entropy. *J. Sound Vib.* **2015**, *339*, 419–432. [CrossRef]
13. Li, D.; Kuang, K.; Koh, C. Rail crack monitoring based on Tsallis synchrosqueezed wavelet entropy of acoustic emission signals: A field study. *Struct. Health Monit.* **2018**, *17*, 1410–1424. [CrossRef]
14. Zhang, X.; Feng, N.; Zou, Z.; Wang, Y.; Shen, Y. An investigation on rail health monitoring using acoustic emission technique by tensile test. In Proceedings of the 2015 IEEE International Instrumentation and Measurement Technology Conference (I2MTC) Proceedings, Pisa, Italy, 11–14 May 2015; pp. 1046–1051. [CrossRef]
15. Wang, J.; Liu, X.-Z.; Ni, Y.-Q. A Bayesian Probabilistic Approach for Acoustic Emission-Based Rail Condition Assessment. *Comput.-Aided Civ. Infrastruct. Eng.* **2017**, *1*, 21–34. [CrossRef]
16. Zhang, X.; Wang, K.; Wang, Y.; Shen, Y.; Hu, H. An improved method of rail health monitoring based on CNN and multiple acoustic emission events. In Proceedings of the 2017 IEEE International Instrumentation and Measurement Technology Conference (I2MTC), Turin, Italy, 22–25 May 2017; pp. 1–6. [CrossRef]
17. Li, D.; Wang, Y.; Yan, W.-J.; Ren, W.-X. Acoustic emission wave classification for rail crack monitoring based on synchrosqueezed wavelet transform and multi-branch convolutional neural network. *Struct. Health Monit.* **2020**, *20*, 1563–1582. [CrossRef]
18. Zhang, X.; Wang, K.; Wang, Y.; Shen, Y.; Hu, H. Rail crack detection using acoustic emission technique by joint optimization noise clustering and time window feature detection. *Appl. Acoust.* **2020**, *160*, 107141. [CrossRef]
19. Bollas, K.; Papasalouros, D.; Kourousis, D.; Anastasopoulos, A. Acoustic emission monitoring of wheel sets on moving trains. *Constr. Build. Mater.* **2013**, *48*, 266–1272. [CrossRef]
20. Kostryzhev, A.; Davis, C.; Roberts, C. Detection of crack growth in rail steel using acoustic emission. *Ironmak. Steelmak.* **2013**, *40*, 98–102. [CrossRef]
21. Li, D.; Kuang, K.; Koh, C. Fatigue crack sizing in rail steel using crack closure-induced acoustic emission waves. *Meas. Sci. Technol.* **2017**, *28*, 065601. [CrossRef]
22. Hase, A.; Mishina, H.; Wada, M. Correlation between features of acoustic emission signals and mechanical wear mechanisms. *Wear* **2012**, *292–293*, 144–150. [CrossRef]
23. Hase, A. Early Detection and Identification of Fatigue Damage in Thrust Ball Bearings by an Acoustic Emission Technique. *Lubricants* **2020**, *8*, 37. [CrossRef]
24. Pollock, A. Acoustic Emission Inspection, Metals handbook. *ASM Int.* **1989**, *17*, 278–294.
25. Chen, Y.; Gou, B.; Yuan, B.; Ding, X.; Sun, J.; Salje, E.K.H. Multiple Avalanche Processes in Acoustic Emission Spectroscopy: Multibranching of the Energy−Amplitude Scaling. *Phys. Status Solidi. B* **2022**, *259*, 2100465. [CrossRef]
26. Chen, Y.; Ding, X.; Fang, D.; Sun, J.; Salje, E.K.H. Acoustic Emission from Porous Collapse and Moving Dislocations in Granular Mg-Ho Alloys under Compression and Tension. *Sci. Rep.* **2019**, *9*, 1330. [CrossRef]
27. Ono, K.; Yamamoto, M. Anisotropic mechanical and acoustic emission behavior of A533B steels. *Mater. Sci. Eng.* **1981**, *47*, 247–263. [CrossRef]
28. Barat, V.; Marchenkov, A.; Bardakov, V.; Zhgut, D.; Karpova, M.; Balandin, T.; Elizarov, S. Assessment of the Structural State of Dissimilar Welded Joints by the Acoustic Emission Method. *Appl. Sci.* **2022**, *12*, 7213. [CrossRef]
29. Chen, G.; Luo, H.; Yang, H.; Han, Z.; Lin, Z.; Zhang, Z.; Su, Y. Effects of the welding inclusion and notch on the fracture behaviors of low-alloy steel. *J. Mater. Res. Technol.* **2019**, *8*, 447–456. [CrossRef]
30. Vinogradov, A.; Merson, D. The Nature of Acoustic Emission during Deformation Processes in Metallic Materials. *Low Temp. Phys.* **2018**, *44*, 930–937. [CrossRef]
31. Kumar, J.; Sarmah, R.; Ananthakrishna, G. General Framework for Acoustic Emission during Plastic Deformation. *Phys. Rev. B* **2015**, *92*, 144109. [CrossRef]